Plasma jet formation and magnetic-field generation in the intense laser plasma under oblique incidence

Y. Sentoku,[a] H. Ruhl,[b] K. Mima, R. Kodama, K. A. Tanaka,[c] and Y. Kishimoto[d]
Institute of Laser Engineering, Osaka University, Suita, Osaka, Japan

(Received 21 December 1998; accepted 8 April 1999)

Long-scale jet-like x-ray emission was observed in the experiments on the interactions of 100 TW laser light with plasmas. The jet formation is investigated by simulations with a two-dimensional particle code. When an *S*-polarized intense laser is irradiated obliquely on an overdense plasma, collimated MeV electrons are observed from the critical surface in the specular reflection direction. These electrons are found to be accelerated through the coronal plasma by the reflected laser light, which was modulated at the reflection point. The quasisteady magnetic channel occurs simultaneously and collimates the energetic electrons along the specular direction. In the case of *P*-polarized laser, it is found that an outgoing electron stream is induced at the critical surface due to Brunel mechanism. Megagauss quasistatic magnetic fields are generated and pinch the electron stream. The angle of ejected electron depends on the electron's energy. The emission direction of the jet generated by the *P*-polarized light is determined by the canonical momentum conservation along the target surface. © *1999 American Institute of Physics.* [S1070-664X(99)03207-3]

I. INTRODUCTION

The interaction of the ultra intense laser with dense plasmas are being widely investigated in relation to the fast ignitor scheme for inertial confinement fusion. Especially, the relativistic intense laser pulse propagation in under dense plasma, the generation of MeV electrons and megagauss magnetic fields are hot topics. Recently, megagauss magnetic fields and a high-energy density plasma jet have been observed experimentally on solid targets irradiated by an ultraintense laser pulse.[1] Two-dimensional (2D) magnetohydrodynamic simulations were performed to reproduce the experimental features and the jet formation by the magnetic fields.[1] And, the generation of quasistatic magnetic fields for the case of oblique incidence was also studied analytically and numerically.[2]

Furthermore, a sharply collimated energetic electron jets is also observed in the interaction of a *P*-polarized intense laser with a steep density profile plasma by S. Bastiani *et al.*[3] A long-scale jet-like x-ray emission was observed in our experiments of 100 TW laser light[4] as shown in Fig. 1. The detailed experimental parameters and conditions were given in Ref. 4. In this experiments, the preformed plasma was generated by 0.3 TW/100 ps laser light on the target surface. The 100 TW/0.5 ps laser light was irradiated normally on the preformed plasma. A hot spot was observed on the target surface, where the position is far from the beam axis. The incident laser appears to be reflected at the top of the preformed plasma in the direction perpendicular to the polarization, namely, the reflected light is *S*-polarization. The jet-like emission was well collimated and continued almost 4 mm from the target surface in the specular direction of the reflected laser light. The analysis of this jet-like emission is the main purpose of this paper. We studied the interactions of obliquely incident *S*-polarized and *P*-polarized lasers with dense plasmas which have a large-scale low-density profile with a plasma corona by using an electromagnetic, relativistic 2D particle-in-cell (PIC) simulation code. In our previous work, high current electron jets from the irradiated plasma surface have been observed by the PIC and an 2D Vlasov simulation code where the boosting frame was applied to simulate under oblique incidence for *P*-polarized lasers.[5]

In this paper, we demonstrate that the both *S*- and *P*-polarized lasers generate energetic electron jets and create megagauss magnetic fields in the coronal plasma. Although the electron acceleration mechanisms are different for the *S*- and *P*-polarization. Hot electron jets penetrating into the overdense plasma are also discussed for an interest in the fast ignition scheme. This paper is organized as follows: The laser irradiation conditions and plasma parameters of 2D PIC simulation are explained in Sec. II. The results of simulations for *S*-polarized and *P*-polarized laser are discussed in Secs. III and IV, respectively. Finally, Sec. IV is devoted to the discussion and conclusion.

II. TWO-DIMENSIONAL PIC SIMULATION FOR OBLIQUE INCIDENCE

The formation of electron jets and quasistatic magnetic fields under oblique incidence are investigated with a 2D PIC code. The geometry of the simulations is shown in Fig. 2. The simulation system size is 23 μm square and the plasma width is 13.5 μm and the maximum density is four times critical density. The plasma consists of fully ionized deuterium (ion mass is $3680m_e$), and the initial electron and ion

[a]Electronic mail: sentoku@ile.osaka-u.ac.jp
[b]Theoretische Quantenelektronik, TH-Darmstadt, Darmstadt, Germany.
[c]Department of Electromagnetic Energy Engineering and Institute of Laser Engineering, Osaka University, Suita Osaka, Japan.
[d]Japan Atomic Energy Research Institute, Naka-machi, Naka-gun, Ibaraki, Japan.

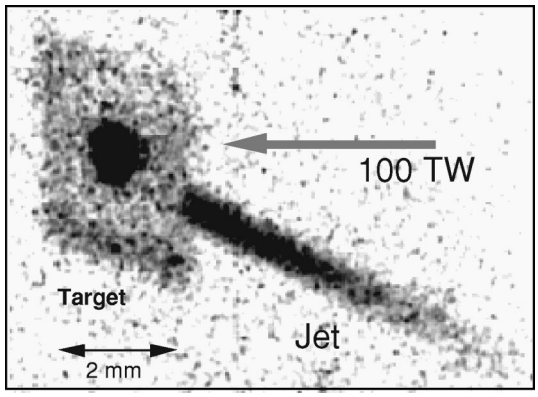

FIG. 1. X-ray image from the target rear side with a large aperture pinhole camera. A mm-scale jet-like emission was observed.

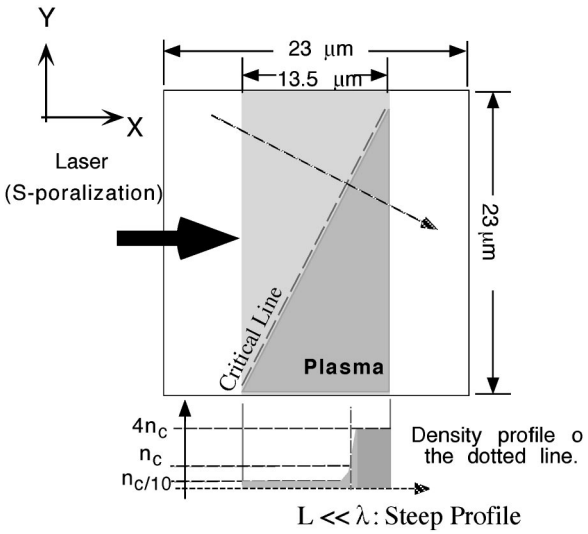

FIG. 2. The geometry of 2D PIC simulation. The plasma has a steep density profile and an oblique surface at critical density. The laser is coming from the left side and the incident angle is equal to 28.9 °.

temperature are 8 and 80 eV, respectively. The plasma surface is oblique where the plasma density changes from $0.1n_c$ to $4n_c$. The density decreases exponentially within 0.2 μm, from $4n_c$ to $0.1n_c$. A uniform coronal plasma, whose density is $0.1n_c$, is put in front of the critical surface. The laser wavelength λ and the intensity are 1 μm and 2×10^{18} W/cm^2, respectively. Thus, the density scale length is less than the wavelength λ, $L=n_e(dn_e/dx)^{-1}\ll\lambda$. The *S*- or *P*-polarized laser is irradiated from the left boundary. The incident angle is set at 28.9 °. The laser intensity increases with a half-Gaussian pulse of 25 fs rise-time and is kept constant after 25 fs. The transverse profile is also Gaussian and the spot size (full width of half maximum) is 7 μm. The peak plasma density is 4.46×10^{21} cm^{-3}, which correspond to $4n_c$. In the *Y* direction, the system is the periodic. In the *X* direction, an absorbing boundary is assumed for the fields. The particles are assumed reflected with the initial thermal

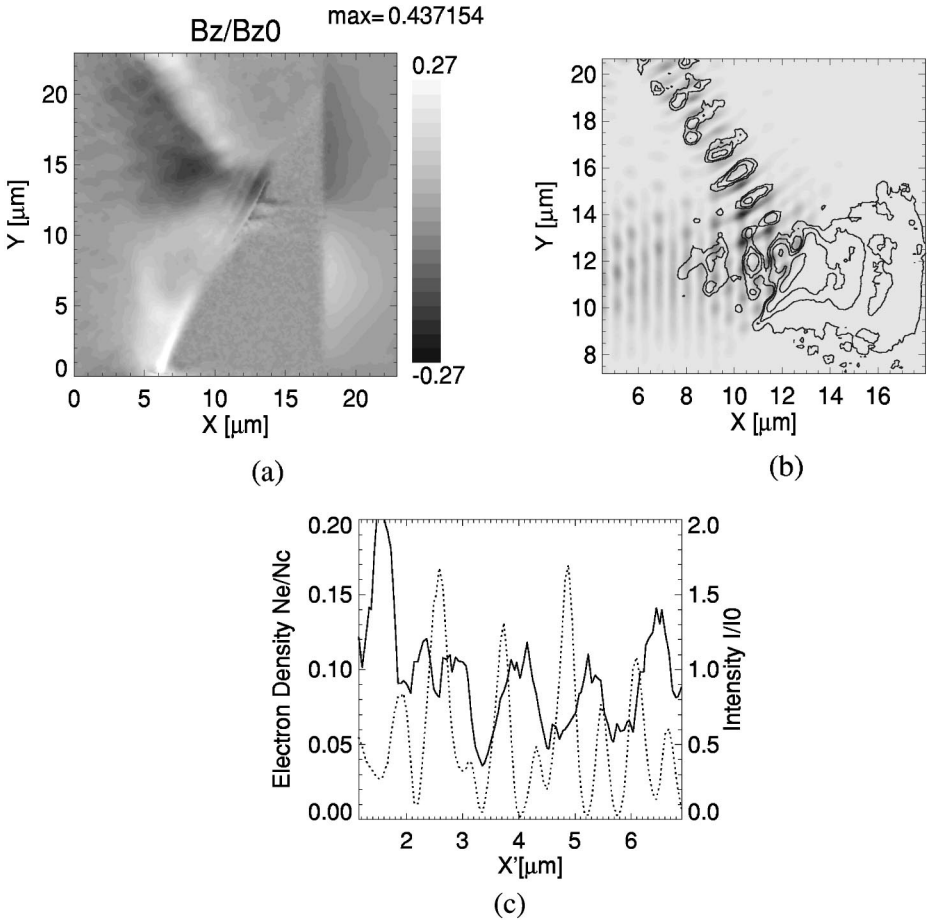

FIG. 3. The quasistatic magnetic fields (a) and the instantaneous laser intensity contours are over-plotted with the electron energy density (b) at 200 fs. Plot (c) is the electron density (solid line) and the laser intensity (dotted line) in the specular direction.

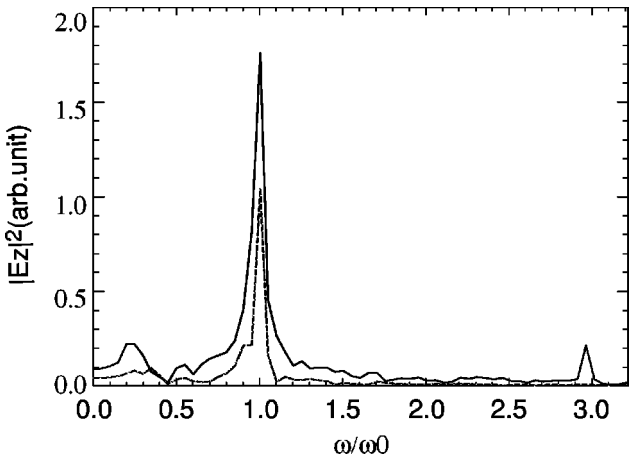

FIG. 4. The spectrum of reflected laser light at 160 fs, which was observed at ($X=10\ \mu$m, $Y=15.7\mu$m). The dotted line is the spectrum of the incident light at 60 fs.

velocity at the X boundaries. The number of spatial grids and particles are 512×512 and 1.22×10^7, respectively.

III. JETS FROM *S*-POLARIZATION LASER

The simulation results for *S*-polarized laser are discussed in this section. Figures 3(a) shows the quasistatic magnetic fields at 200 fs. The magnetic fields are normalized by the incident laser field B_{z0} ($\sim$100 MG). The quasistatic magnetic fields are excited along the specular direction and their intensities reach about 20 MG. Figures 3(b) shows that the instantaneous laser intensity contours are over plotted together with the electron energy density. The electron jets are observed in completely specular direction in this case, and also the energetic electrons penetrate into the overdense plasma in the incident laser direction as shown in Fig. 3(b). Figure 3(c) shows a plot of the electron density on the specular reflection direction at 200 fs. $X''=0$ denotes the reflection point. Plasma waves are excited by the modulated laser light as shown in Fig. 3(c). These plasma waves accelerate electrons toward the specular reflection direction. The modulation of the reflected light is clearly seen in the spectrum as shown in Fig. 4, observed in the specular reflection direction at around 160 fs. The reflected laser spectrum is broad and the peak intensity is greater than the initial intensity because of the self-focusing, which is due to the surface deformation and relativistic effects.[2] A large shift towards lower frequencies of the base frequency ω_0 and higher frequencies are observed. The spectrum modulation can be explained by absorption at the reflection point, the absolute Raman scattering, and stimulated forward Raman scattering, as discussed in Ref. 6. This is known as the self modulated laser wake field accelerator.[7,8] The electron acceleration is enhanced by the modulation and self-focusing of the reflected laser light. In the reflected spectrum, the third harmonics are also observed.[9]

The interaction of ultra short laser pulses with a dense plasma at oblique incidence is also studied, since the modulation of the reflected pulse could be seen clearly. Figures 5(a) shows temporal evolution of intensity of the laser pulse at 20, 40, and 80 fs, where the initial pulse length is about 20 fs. It was observed that the reflected pulse is focused and modulated along the propagation direction. Electrons are trapped in the pulse and accelerated to over MeV energy as shown in Figs. 5(b), which is the electron energy density at 80 fs. Also these electrons are pinched by self excited quasistatic magnetic fields. The electron density is shown in Figs. 5(c), the excited wake fields are observed along the incident axis and the modulated wake fields are also observed in the specular direction.

IV. JETS FROM *P*-POLARIZATION LASER

In this section, we discuss the results of *P*-polarized laser. Note that, the temporal evolution is significantly different from that of the *S*-polarization case. Namely, the stationary electron jets begin to be observed after 100 fs. On the other hand, the electron jets and the quasistatic magnetic fields built up very quickly, in only several tens fs after laser irradiation begins. Figures 6(a) and 6(b) show the quasistatic magnetic fields B_z and the instantaneous electron energy density at 120 fs. All parameters are the same as Fig. 3, except the polarization. The strong bipolar magnetic fields are built up in front of the critical surface and extended to the end of the plasma corona. The maximum amplitude is reached to about 60 MG. This bipolar magnetic fields have an opposite polarity with the fields which generated by the fast electrons accelerated into the overdense plasma by the ponderomotive force.[10,11] The observed quasistatic magnetic fields are not symmetrical on the critical surface, the positive magnetic field extends along the surface, implying the dc surface currents, which was mentioned in Ref. 2. These magnetic fields are induced by the high-energy currents from the critical surface, which are observed in Figs. 6(b). Also high energetic electrons penetrate into the overdense plasma. These electrons run mainly toward target normal direction and split into filaments in the overdense region. These current filaments are correlated with the magnetic filaments observed in overdense region, as shown in Figs. 6(a).

Figure 6(b) shows the instantaneous plot of the electron energy density with positive laser field B_z (dotted line). It is clearly seen that the outgoing electrons are extracted once in the laser oscillating period from the critical surface by the Brunel absorption,[12] since the electron bunch length is almost equal to the laser wavelength. The average energy of bunched electrons is about $1.5\,\mathrm{MeV}(\gamma\simeq3)$. The energetic electrons, which are pinched by the quasistatic magnetic fields, move along the magnetic corridor, whose direction is close to the laser specular reflection direction. More precisely, the direction of the jet is different from the specular reflection direction. The specular reflection angle is 28.9° with respect to the target normal but the collimated electron jet is observed at about 17°. Here, we estimate the direction of the outgoing electron jets. The specular direction θ and the angle of electron jets θ' as shown in Fig. 7. The photon momentum of the laser and the momentum of electron are $\hbar k$ and p, respectively. The momentum components parallel to the plasma surface are given by $k_\parallel$ and $p_\parallel$ for laser and

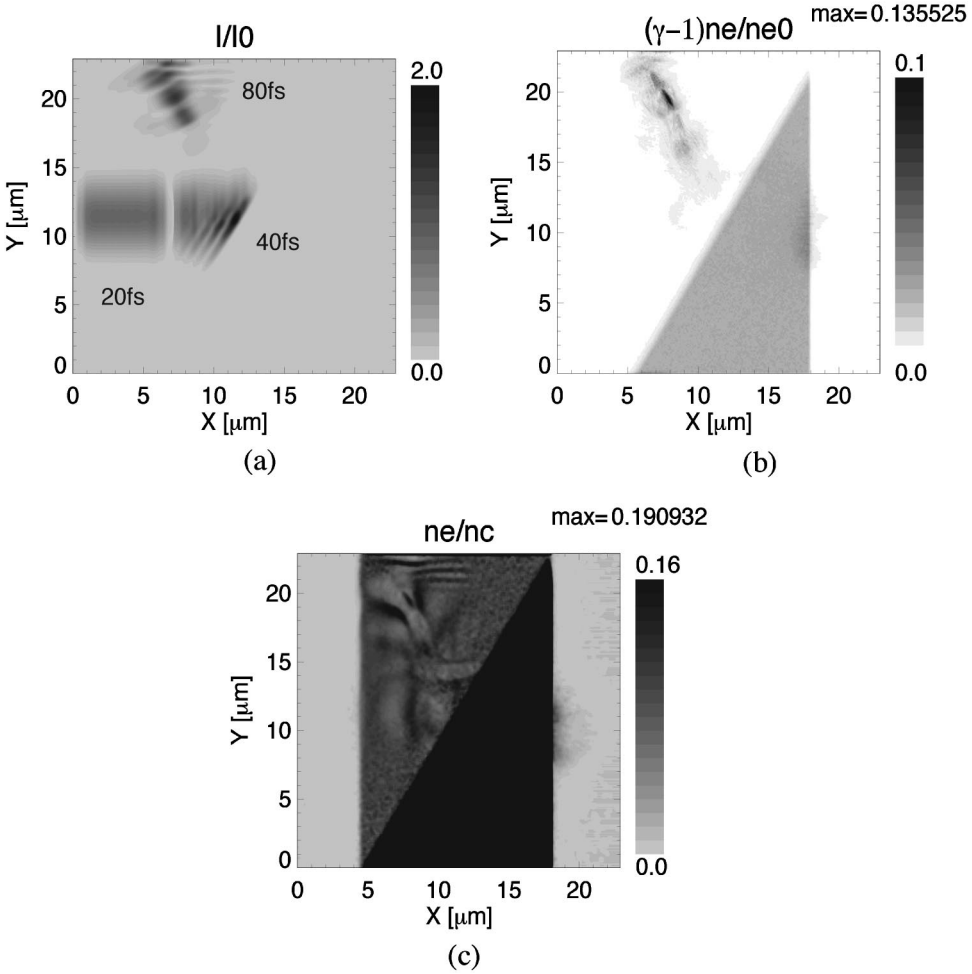

FIG. 5. The results of *S*-polarized ultra short laser pulse. The temporal evolution of the intensity of laser pulse is shown in plot (a). The electron energy density and the electron density at 80 fs are shown in (b) and (c), respectively. All plots are time averaged a period of the laser light.

electron, respectively. Then θ and θ' are given by the following relations:

$$\sin\theta = \frac{k_{\parallel}}{k}, \quad \sin\theta' = \frac{p_{\parallel}}{p}. \tag{1}$$

For simplicity, it is assumed that the initial electron has no kinetic energy, and the plasma surface is flat. Thus, the total canonical momentum of electron and photon is conserved along this surface. During the interaction with the laser fields, the electron kinetic energy increases to $(\gamma-1)m_e c^2$.

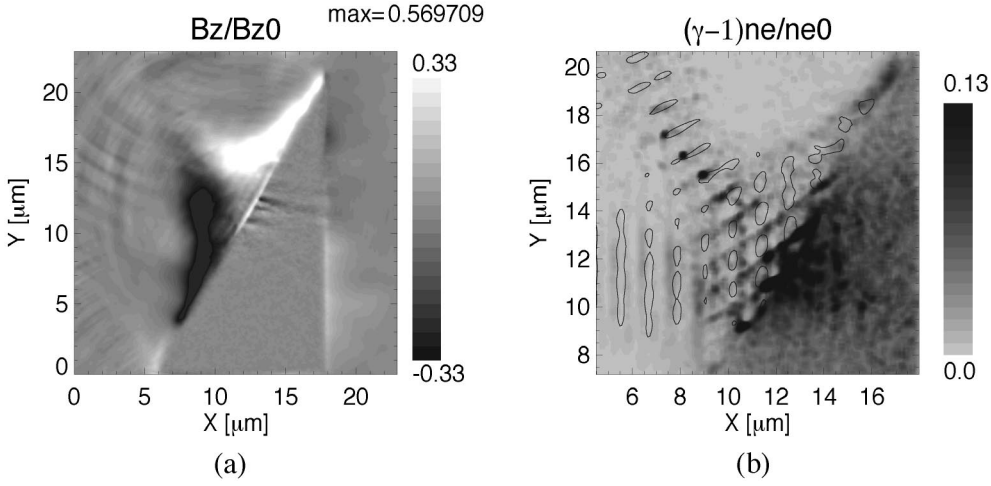

FIG. 6. The laser is *P*-polarized and the other parameters are the same as Fig. 3. The plot of quasistatic magnetic field (a) at 120 fs. The asymmetry on the surface indicates the surface currents and the intensity of quasistatic magnetic fields are up to 50 MG. The instantaneous plot of the electron energy density (b), the positive fields of the *p*-polarized laser (B_z) are over-plotted (dotted line). High-energy electrons are extracted once per laser period from the plasma surface and pinched by the quasistatic magnetic fields. The electron's energy is in excess of 1 MeV and the ejection angle is 16.7°.

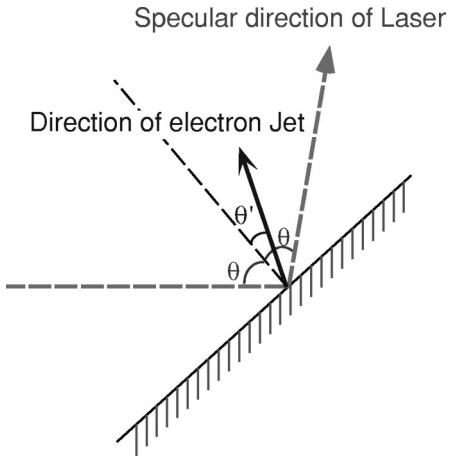

FIG. 7. The definition of two angles. The angle of electron jets θ' is always smaller than the angle of specular direction θ.

The component of the total canonical momentum along the surface $N_e p_\parallel + \hbar k_\parallel N_p$ is always conserved[2,5] for each accelerated electron, where N_e and N_p are electron density and photon density. Therefore, the absorbed photon momentum along the surface is equal to the electron momentum. The number of the interacted photons per electron, N_p/N_e is estimated as $N_p/N_e=(\gamma-1)m_e c^2/\hbar\omega$, so the parallel component of the momentum along the surface is given by

$$p_\parallel=\frac{N_p}{N_e}\hbar k_\parallel=(\gamma-1)m_e c\frac{k_\parallel}{k}=(\gamma-1)m_e c\sin\theta. \tag{2}$$

Then, the angle of outgoing direction θ' is given as following:

$$\sin\theta'=\frac{p_\parallel}{p}=\frac{\gamma-1}{\gamma}\sin\theta. \tag{3}$$

Here, the total momentum of electron is given by $p\simeq\gamma m_e c$ in the relativistic regime. So when an electron is accelerated to strongly a relativistic energy, θ and θ', will be close. In contrast, the nonrelativistic electrons are emitted toward target normal direction, since $(\gamma-1)/\gamma\ll 1$. In this simulation, the averaged energy of bunched electrons is about 1.5 MeV($\gamma\simeq 3$) and the estimated θ' from Eq. (3) is about 18°. This agrees with the angle of electron jets observed at 120 fs in 2D PIC simulation.

Figures 8(a) and 8(b) show the quasistatic magnetic fields and the electron jets in the case of the strong relativistic laser intensity, 2×10^{19} W/cm^2. Both plots are time averaged over a laser oscillating period. The quasistatic magnetic fields are growing up to 250 MG, and the electrons' averaged energy reached $\gamma\simeq 6$. The angle of jets from Eq. (3) is 28.2°, close to the specular direction. This angular dependence is well reproduced in the simulation as shown in Fig. 8(b). In the case of no coronal plasma, the electron jets are never observed and the magnetic fields are localized on the critical surface and cannot extend to outside like Fig. 6(a). These facts indicate that a low density plasma corona plays an important role in the generation of outgoing electron jets and the quasistatic magnetic fields.

V. DISCUSSIONS AND CONCLUSIONS

The absorption efficiencies of *P*- and *S*-polarized laser for 2×10^{18} W/cm^2 are 26% and 7.8%, respectively. Thus the absorption of *P*-polarized laser light is three times greater than for the *S*-polarized light. There is the important difference of the angle of the in-going fast electrons, which penetrate into the overdense region. To see the direction of the in-going electron jets clearly, the hard x-ray emissions from the hot electrons are evaluated using the bremsstrahlung model in 2D PIC simulation.[13] In this model, the relativistic bremsstrahlung cross section is based on the quantum electrodynamics and integrated by the Monte Carlo method. Reference 13 shows that the emission of hard x-ray photons is strongly collimated in the direction of electron motion, when the electron has relativistic energy. The calculated energy range of the hard x-ray photons is from 1 to 10 MeV. The obtained angular distributions of total emission power are shown in Fig. 9(a) for *P*-, and Fig. 9(b) for *S*-polarized laser

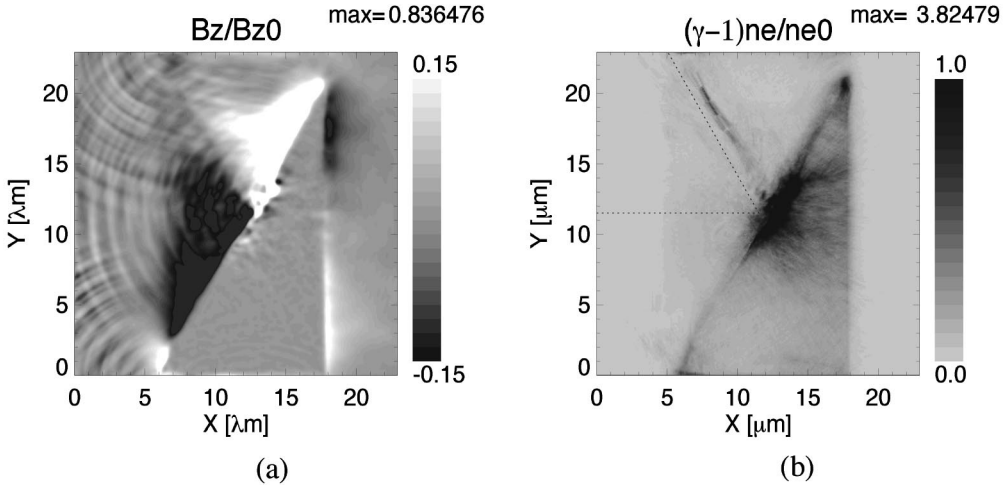

FIG. 8. The quasistatic magnetic field (a) and the electron energy density (b) at 120 fs, when the intensity of *P*-polarized laser is in the strong relativistic regime, 10^{19} W/cm^2. Both plots are averaged over a laser oscillating period. The average energy of electrons is over 2.5 MeV($\gamma\simeq 6$) and the estimated angle is 28.2°, close to the specular direction.

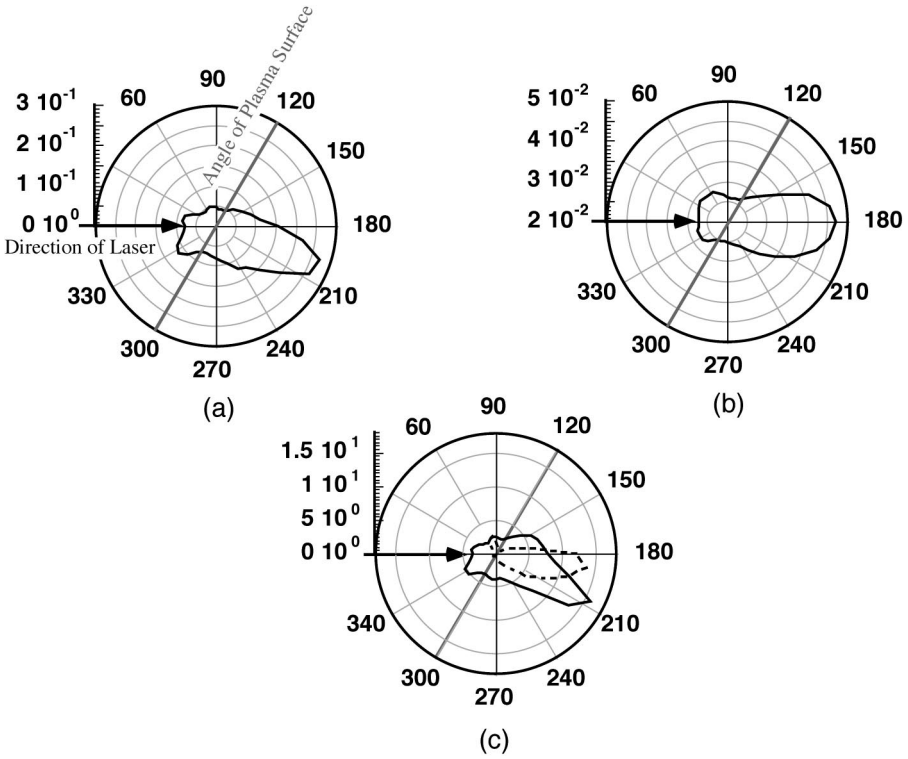

FIG. 9. The angular distribution of the power of hard x-rays. These plots are in the unit $[10^{-29}/(Z^2 n_i n_e)]\,\mathrm{W\cdot cm^3}$. Plots (a) and (b) are the total emission in the case of *P*-polarized and *S*-polarized laser through 200 fs, respectively. The total emission power of *P*-polarized is three times greater than that of *S*-polarized laser light. Plot (c) is for the case the relativistic laser intensity $2\times10^{19}\,\mathrm{W/cm^2}$ of *P*-polarized at 200 fs. In plot (c), the dotted line is the result at 50 fs and it has been scaled up by a factor of 50 for the overplot.

through simulation. Figure 9(c) is for the relativistic intensity of *P*-polarized light. In these polar plots, the incident direction of the light is 180°, the specular reflection direction is about 60° and the target normal direction is about 30°. The emission is collimated in the incident laser axis for *S*-polarized light as shown in Fig. 9(b), since the electrons are accelerated only by $J\times B$ force. The total emission power of *S*-polarized is about three times smaller than the case of *P*-polarized light, which corresponds to the absorption efficiency. On the other hand, the emission is toward the target normal direction for the *P*-polarized laser, especially the relativistic intensity as shown in Figs. 9(a) and 9(c). Figure 9(c) shows that the electrons are accelerated close to the laser direction in the early time (50 fs). So the electrons are mainly accelerated by the laser fields, $J\times B$ force at this moments. Figure 10 shows that the spectrum of the fluctuation of the charge density ρ, namely the plasma wave at the reflection point. The plasma wave is driven by the normal component of the laser field, whose oscillating frequency is ω_0. The excited spectra of plasma waves, $0.1\omega_0, \omega_0, 2\omega_0, 3\omega_0, 4\omega_0$, are clearly observed at 120 fs (solid line). But no significant spectra of plasma waves at 40 fs (dotted line). These results indicate that the electrons are pushed toward target normal direction by the electrostatic potential at the surface after the plasma waves are excited. When this plasma wave acceleration is dominant, the fast electrons mainly penetrate into the overdense plasma toward target normal direction, especially when the laser intensity is in the relativistic regime. This is a quite useful feature for the fast ignitor scheme.

We demonstrate the plasma jets formation and magnetic-field generation in the obliquely incident laser produced plasmas using the 2D PIC code, which includes the hard x-ray emissions. In the case of *S*-polarized light, the electrons accelerated by the plasma wave driven by the modulated reflected laser pulses, and this electron jets continue to the end of the plasma corona and is guided by the quasistatic magnetic fields. This electrons jet corresponds to the long-scale jet, which was observed at 100 TW laser plasma interactions. *P*-polarized laser also generates electrons jets by vacuum heating and megagauss quasistatic magnetic fields. The conditions of simulation which we performed are the best ones to see the specular jets, especially the density scale length. When the plasma has a long scale density profile, the interaction surface is deformed and corrugated and no clear jets were observed. We found that the coronal plasma plays an important role in forming the electron jets; without it no specular jets are observed.

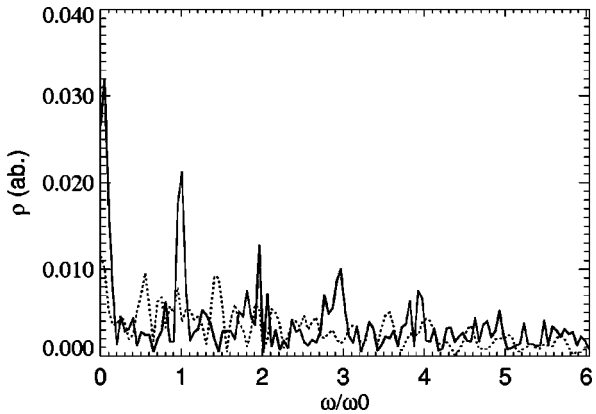

FIG. 10. The spectrum of the fluctuation of the charge density on the reflection point at about 40 fs (dotted line) and 120 fs (solid line). The parameters are the same as Fig. 9(c).

[1]M. Borghesi, A. J. MacKinnon, A. R. Bell, R. Gaillard, and O. Will, Phys. Rev. Lett. **81**, 112 (1998).
[2]V. A. Vshivkov, N. M. Naumova, F. Pegoraro, and S. V. Bulanov, Phys. Plasmas **5**, 2727 (1998).
[3]S. Bastiani, A. Rousse, J. P. Geindre, P. Audebert, C. Quoix, G. Hamoniaux, A. Antonetti, and J.-C. Gauthier, Phys. Rev. E **56**, 7179 (1997).
[4]R. Kodama, K. A. Tanaka, Y. Sentoku, T. Matsushita, K. Takahashi, Y. Kato, H. Fujita, Y. Kitagawa, T. Kanabe, T. Yamanaka, and K. Mima, Phys. Rev. Lett. (submitted).
[5]H. Ruhl, Y. Sentoku, K. Mima, K. A. Tanaka, and R. Kodama, Phys. Rev. Lett. **82**, 743 (1999).
[6]S. V. Bulanov, N. M. Naumova, and F. Pegoraro, Phys. Plasmas **1**, 745 (1994).
[7]E. Esarey, J. Krall, and P. Sprangle, Phys. Rev. Lett. **72**, 2887 (1994).
[8]S. Kato, Y. Kishimoto, and J. Koga, Phys. Plasmas **5**, 292 (1998).
[9]R. Lichiters, J. Meyer-ter-Vehn, and A. Pukhov, Phys. Plasmas **3**, 3425 (1996).
[10]R. N. Sudan, Phys. Rev. Lett. **70**k, 3075 (1993).
[11]S. C. Wilks, W. L. Kruer, M. Tabak, and A. B. Langdon, Phys. Rev. Lett. **69**, 1383 (1992).
[12]F. Brunel, Phys. Rev. Lett. **59**, 52 (1987).
[13]Y. Sentoku, K. Mima, T. Taguchi, S. Miyamoto, and Y. Kishimoto, Phys. Plasmas **5**, 4366 (1998).